Thermal decomposition of ammonium tetrathiotungstate

Dávid Hunyadi[1], Ana Luisa Vieira Machado Ramos[1,2], Imre Miklós Szilágyi[1,3]

[1]Department of Inorganic and Analytical Chemistry, Budapest University of Technology and Economics, H-1111 Budapest, Szt. Gellért tér 4. Hungary
[2]Department of Mining Engineering, Federal University of Minas Gerais, 31270-901 Belo Horizonte, Av. Antônio Carlos 6627. Brazil
[3]Technical Analytical Chemistry Research Group of the Hungarian Academy of Sciences, Budapest University of Technology and Economics, H-1111 Budapest, Szt. Gellért tér 4. Hungary
Corresponding author: imre.szilagyi@mail.bme.hu

Keywords

$(NH_4)_2WS_4$, WS_3, WS_2, WO_3, TG/DTA, MS, XRD, FTIR, SEM

Abstract

The thermal decomposition of ammonium tetrathiotungstate (ATT), $(NH_4)_2WS_4$ was studied by SEM, FTIR, XRD, EDX and TG/DTA-MS. The decomposition of ATT involved three steps in inert atmosphere: (i) release of free water between 30-140 °C; (ii) formation of an amorphous WS_3 phase between 170-280 °C, from which (iii) a slightly crystalline WS_2 formed between 330-470 °C. As a difference compared to inert atmosphere, in air in the second step the ATT decomposed into directly WS_2 instead of WS_3. This WS_2 phase was amorphous, and still contained traces of ATT. Between 260-

500 °C from the WS_2 monoclinic tungsten oxide crystallized in two steps: at 302 °C a slightly crystalline m-WO_3 formed, which became more crystalline at 471 °C. During the investigation of the effect of the particle size, it was found that the thermal behaviour of ATT crystals was similar to ATT powder, with some shift in the decomposition temperature. The XRD results showed that the WS_2 formed from the ATT powder in N_2 had a higher level of crystallization, compared to the WS_2 obtained from ATT crystals.

1. Introduction

Ammonium tetrathiotungstate (ATT, $(NH_4)_2WS_4$) is an important material as a precursor for WS_3 [1-4], WS_2 [4-11] and different tetraalkylammonium thiotungstates [7, 12-17]. ATT is an important industrial lubricant as-well [18]. Tetraalkylammonium thiotungstates are precursors for WS_2 catalysts [7, 15-17]. WS_2 can be also used as gas sensor [6,19-20], dry lubricant [21,22] and in lithium batteries [23-25].

WS_2 catalysts are promoted mostly with cobalt or nickel and used in hydrodesulfurization (HDS) reactions [26-28]. HDS is the central process to remove sulphur from crude oils. There are several ways to prepare these catalysts, like comaceration [29], homogeneous sulphide precipitation [14], hydrothermal and solvothermal processes [30-34], solution reactions [35,36] and thiosalt decomposition [37-39]. With the decomposition of thiotungstates a high sulphur content can be achieved in the final WS_2 catalysts [40,41]. Also the controlled composition and wide ranges of achievable surface areas [6,42-45] made this method promising for preparing WS_2 catalysts. The thiotungstate precursors can be activated by ex situ or in situ methods. The ex situ method means, that the precursor is activated under a H_2/H_2S gas flow, by heating it to 400 °C with 4 °C min^{-1}, and then keeping the material at this temperature for 4 h. In situ activated catalysts are prepared by thermal decomposition of the precursors at 350 °C with 10 °C min^{-1}, 3.1 MPa in H_2 atmosphere [5].

Because of the importance of these preparation methods, it is crucial to have detailed knowledge the thermal decomposition of the various thiotungstate precursors. The thermal behaviour of different tetraalkylammonium thiotungstates was investigated previously in detail [7,9,10,15,16,39,46-48], but in case of the ATT only some studies can be found [5,49,50]. In 1970 Voorhoeve et al [49] investigated the decomposition of ATT in vacuum and H_2 flow by X-ray diffraction (XRD), differential thermal analysis (DTA), optical microscopy and electron spin resonance (ESR). The results showed that ATT decomposed in two steps, and the temperature of the steps depended on the pressure, but did not depend on the particle size in the 50-2000 μm range. In the first step (ca. 120-300 °C) an amorphous

tungsten sulfide phase formed in an endothermic process with a composition of $WS_{2.6-3.3}$, which crystallized into WS_2 at 300-400 °C in an exothermic process.

The other two studies are more recent. Espino et al. [5] characterized the decomposition in N_2 flow with thermogravimetric (TG), and DTA measurements. Their results also showed that ATT decomposed in two steps. The first step occurred at ca. 190-280 °C when WS_3 was formed in an endothermic reaction, and NH_3 and H_2S evolved in this step. Then at ca. 340-410 °C the as-formed WS_3 decomposed into WS_2 in an exothermic reaction. The composition of the annealing products and the quality of the evolved gases were calculated from the experimental mass losses.

Yi et al. investigated the decomposition of ATT in N_2 as well by TG, temperature-programmed decomposition with mass spectroscopy (TPD-MS), in situ FTIR and Raman spectroscopic measurements [50]. In the first step (175-250 °C) WS_3 formed, while H_2O, H_2 and NH_3 evolved, then at 350-400 °C WS_2 formed accompanied with the loss of sulphur.

The need for our research was that, to best to our knowledge, there had been no previous detailed study on the thermal behaviour of ATT in air. In this study we aimed to get more information on the thermal decomposition of ATT both in air and in inert atmospheres, characterize the intermediates and investigate the effect of the particle size of ATT. For this thermal analysis (TG/DTA-MS), powder X-ray diffraction (XRD), Fourier transform infrared spectroscopy (FTIR), scanning electron microscopy (SEM) and energy-dispersive X-ray spectroscopy (EDX) were used.

2. Experimental

The ATT material was obtained from Alfa-Aesar, which had the composition of $(NH_4)_2WS_4$ (CAS:13862-78-7).

SEM images and EDX data were obtained by a JEOL JSM-5500LV scanning electron microscope.

Powder XRD patterns were recorded on a PANalytical X'pert Pro MPD X-ray diffractometer using Cu K_α radiation.

FTIR spectra were measured by an Excalibur Series FTS 3000 (Biorad) FTIR spectrophotometer in the range of 400-4000 cm^{-1} in KBr pellets.

TG/DTA measurements were performed on an STD 2960 Simultaneous DTA/TGA (TA Instruments Inc.) thermal analyzer using a heating rate of 10 °C min^{-1} and Pt crucibles. The thermobalance was purged either with air or nitrogen (130 ml min^{-1}). Evolved gas analytical (EGA) curves were recorded by a Thermostar GSD 200 (Balzers Instruments) quadrupole mass spectrometer (MS). A mass range between m/z = 1-64 was monitored through 64 channels in Multiple Ion Detection Mode (MID) with a

measuring time of 0.5 s channel^{-1}. Further details of the TG/DTA-MS setup are described elsewhere [51,52]

3. Results and discussion

3.1 Characterization of the ATT material

According to the SEM images the ATT material was built up mainly by ca. 200-500 μm plain crystals (Fig. 1.A), while there were some larger, ca. 2.5 mm crystals as well (Fig. 1.B). In the FTIR spectrum of ATT (Fig. 2) the O-H deformation and stretching vibrations of the water molecules absorbed on the surface of ATT were present around 1636 cm^{-1} and 3215 cm^{-1} respectively, while the N-H deformation and stretching vibrations of the NH_4^+ ions were visible at 1390 cm^{-1} and 3120 cm^{-1} respectively [50]. The peak at 850 cm^{-1} was assigned to the W=S vibration, and the peak at 460 cm^{-1} to the W-S vibration [47].

In order to investigate the effect of the particle size some of the ATT was powdered. The ATT powder was identified with powder XRD measurement (Fig. 3), and the result was identical to the PDF 076-0751 card. According to the SEM images the ATT powder consisted of ca. 0,5-3 μm particles (Fig. 1.C), which aggregated into larger, 20-40 μm blocks (Fig. 1.D).

3.2 Thermal decomposition of the ATT powder in nitrogen

The ATT powder decomposed in three steps in nitrogen atmosphere. In the first step (30-140 °C) the mass decrease was 0.3 %, and a small amount of water evolved (Fig. 4). This was physically absorbed water, because there was no change in the XRD pattern (Fig. 3). The water evolution was showed by an endothermic peak at 76 °C, and by the MS curve of 18^+ (H_2O).

The second step occurred at 170-280 °C, with a mass decrease of 18.7 %. This decomposition step was accompanied with an endothermic process and with the release of H_2S and NH_3 (Fig. 4). The MS curves also showed that part of the evolved NH_3 and H_2S combusted, resulting in N_2O (44^+), SO (48^+), SO_2 (64^+) and H_2O (18^+). This combustion was possible, because even in the N_2-purged furnace there were traces of O_2. Previously H_2 evolution was reported instead of H_2S at this temperature range [50], but our results did not confirm this. The FTIR results (Fig. 2) also showed the NH_3 evolution, as the N-H peaks at 1390 cm^{-1} and 3120 cm^{-1} disappeared completely. In this step an amorphous tungsten trisulphide was formed as reported before [5,49]. This amorphous state could be seen from the XRD

pattern (Fig. 3) as well. The composition of this phase was close to WS_3, i.e. by TG (Fig. 4) the observed mass loss (18.7 %) was close to the theoretical one corresponding to WS_3 (19.5 %). EDX also confirmed the composition; however, with larger error, as the measured W:S ratio was 1:2.3-3.5 instead of the theoretical 1:3.

In the third step (330-470 °C) the amorphous WS_3 transformed into a slightly crystalline WS_2 (Fig. 3), while sulphur evaporated. The MS curves revealed that the evolved sulphur combusted into SO (48^+) and SO_2 (64^+), the main combustion product being SO_2. The XRD proved the crystallization as at 800 °C a slightly crystalline WS_2 phase was detected. The measured mass loss (27.64 %) was close to the theoretical mass loss corresponding to WS_2 (28.75 %). This transformation was accompanied with an exothermic peak on the DTA curve (Fig. 4), as both the crystallization of WS_2 and the combustion of as-released sulphur are exothermic processes. The transformation into WS_2 could be also seen in the FTIR spectrum, as the region below 1200 cm^{-1} altered significantly (Fig. 2).

3.3 Thermal decomposition of the ATT powder in air

In the first decomposition step (30-120 °C), there was no difference between the thermal behaviour of ATT powder in air and inert atmospheres (Fig. 4-5).

Between 180-260 °C the ATT started to decompose, and similar to the decomposition in nitrogen this step was accompanied by an endothermic process as H_2S and NH_3 were released (Fig. 5). The MS curves showed that some of the H_2S and NH_3 burnt into SO, SO_2 and NO [53-56]. The XRD, FTIR and SEM-EDX results revealed that ATT partially decomposed (only 15.54 % mass loss instead of the theoretical 28.75 %), and from it directly WS_2 was obtained. The XRD pattern showed (Fig. 6) that part of the phase was amorphous WS_2, and also traces of ATT could be found (17.27°, 18.49°, 28.92° and 31.53°). In the FTIR spectrum (Fig. 7), some of the peaks were assigned to the ATT (462 cm^{-1}, 841 cm^{-1} and 1397 cm^{-1}), while the other peaks to the WS_2 (462 cm^{-1}, 516 cm^{-1}, 946 cm^{-1} and 1604 cm^{-1}). On the SEM images it can be seen, that this intermediate contained particles of different sizes. The smallest particles were ca. 1-5 μm, while there were some larger ca. 15-150 μm particles (Fig. 8.A). On the surface of the larger particles there were cracks (Fig. 8.B), which probably formed during gas release. According to the EDX results, most of the smaller particles were WS_2 (W:S ratio 1:2) and the larger particles were ATT (W:S ratio 1:4).

At higher temperature (260-500 °C) the as-obtained intermediate transformed completely into monoclinic tungsten oxide (PDF 89-4476) (Fig. 6). The m-WO_3 crystallized in two steps, at 302 °C a slightly crystalline WO_3 was formed (Fig. 6), which became more crystalline at higher temperature

(471 °C). During this transformation sulphur evaporated, which burnt into SO and SO_2. This transformation was accompanied by a very intense exothermic peak on the DTA curve as both the crystallization and the combustion of the evolved sulphur were exothermic processes.

3.4 Comparison of the thermal behaviour of ATT powder and crystals

The TG/DTA curves of the ATT crystals (Fig. 9) were basically identical to the curves of ATT powder. The mass loss values for ATT crystal and powder in the first, second and third decomposition steps were almost the same. At the second step the decomposition temperature of the powder was lower, than in case of the crystal. On the other hand the decomposition temperature of the third step was not influenced by the particle size.

The FTIR results were identical in case of the powder and crystal. The XRD results were similar too, the only difference was that the WS_2 formed from the ATT powder in N_2 had a higher level of crystallization (Fig. 10).

4. Conclusion

The thermal behaviour of the ammonium tetrathiotungstate was studied by SEM, FTIR, XRD, EDX and TG/DTA-MS.

The thermal decomposition of ATT powder involved three steps in inert atmosphere: (i) release of free water between 30-140 °C, and (ii) formation of an amorphous WS_3 phase between 170-280 °C in endothermic reactions. In this step NH_3 and H_2S evolved, however H_2 evolution could not been detected as written before [50]. Some of the NH_3 and H_2S combusted into H_2O, N_2O, SO and SO_2. (iii) Between 330-470 °C a slightly crystalline WS_2 formed from the WS_3 in an exothermic process. During this process sulphur evaporated, which burnt into SO and SO_2.

As a difference compared to inert atmosphere, in air in the second step an amorphous WS_2 was formed instead of WS_3. This WS_2 phase still contained traces of ATT as-well. Between 260-500 °C from this mixture monoclinic tungsten oxide crystallized in two steps.

The thermal behaviour of ATT crystals was similar to the powder, with some shift in the decomposition temperature. The main difference between them was in the XRD results, which showed that the WS_2 formed from the ATT powder in N_2 had a higher level of crystallization.

5. References

[1] Glemser O, Sauer H, König P. Über Wolframsulfide und wolframselenide. Z Anorg Allg Chem. 1948;257:241-46.

[2] Wildervanck JC, Jellinck F. Preparation and crystallinity of molybdenum and tungsten sulfides. Z Anorg Allg Chem. 1964;328:309-18.

[3] Van der Vlies AJ. Chemical principles of the sulfidation reaction of tungsten oxides. Dissertation, Swiss Federal Institute of Technology Zurich 2002

[4] Ghoreishi SM, Meshkat SS, Dadkhah AA. IF-WS_2 nanoparticles size design and synthesis via chemical reduction. Mater Res Bull. 2010;45(5):584-8.

[5] Espino J, Alvarez L, Ornelas C, Rico JL, Fuentes S, Berhault G, Alonso G. Comparative study of WS_2 and Co(Ni)/WS_2 HDS catalysts prepared by ex situ/in situ activation of ammonium thiotungstate. Catal Lett. 2003;90:71-80.

[6] Zdrazil M. Recent advances in catalysis over sulphides. Catal Today. 1988;3(4):269-365.

[7] Alonso G, del Valle M, Cruz J, Licea-Claverie A, Petranovskii V, Fuentes S. Preparation of MoS_2 and WS_2 catalysts by in situ decomposition of ammonium thiosalts. Catal Lett. 1998;52:55-61.

[8] Pedraza F, Fuentes S. Ni–Mo and Ni–W sulfide catalysts prepared by decomposition of binary thiometallates. Catal Lett. 2000;65:107-13.

[9] Alonso G, Del Valle M, Cruz J, Licea-Claverie A, Petranovskii V, Fuentes S Preparation of MoS_2 catalysts by in situ decomposition of tetraalkylammonium thiomolybdates. Catal Today. 1998;43:117-22.

[10] Alonso G, Petranovskii V, Del Valle M, Cruz-Reyes J, Licea-Claverie A, Fuentes S. Preparation of WS_2 catalysts by in situ decomposition of tetraalkylammonium thiotungstates. Appl Catal A. 2000;197:87-97.

[11] An G, Lu C, Xiong C. Solid-phase reaction synthesis of mesostructured tungsten disulfide material with a high specific surface area. Mater Res Bull. 2011;46(9):1323-6.

[12] McDonald WJW, Delbert Friesen G, Rosehein LD, Newton WE. Syntheses and characterization of ammonium and tetraalkylammonium thiomolybdates and thiotungstates. Inorg Chim Acta. 1983;72:205-10.

[13] Pan WH, Leonowics ME, Stiefel EI. Facile syntheses of new molybdenum and tungsten sulfido complexes. Structure of $Mo_3S_9^{2-}$. Inorg Chem. 1983;22(4):672-678.

[14] Liang KS, Chianelli RR, Chien FZ, Moss SC. Structure of poorly crystalline MoS_2 - A modeling study. J Non-Cryst Solid.(1986;79(3):251-73.

[15] Alonso G, Berhault G, Chianelli RR. Synthesis and characterization of tetraalkylammonium thiomolybdates and thiotungstates in aqueous solution. Inorg Chim Acta. 2001;316:105-9.

[16] Alonso G, Siadati MH, Berhault G, Aguilar A, Fuentes S, Chianelli RR. Synthesis of tetraalkylammonium thiometallate precursors and their concurrent in situ activation during hydrodesulfurization of dibenzothiophene. Appl Catal A. 2004;263:109-17.

[17] Alonso G, Yang J, Siadati MH, Chianelli RR. Synthesis of tetraalkylammonium thiometallates in aqueous solution. Inorg Chim Acta. 2001;325:193-7.

[18] Chinas-Castillo F, Lara-Romero J, Alonso-Núñez G, Barceinas-Sánchez JDO, Jiménez-Sandovale S. Friction reduction by water-soluble ammonium thiometallates. Tribol Lett. 2007;26:137-44.

[19] Hagenbach G, Courty Ph, Delmon B. Physicochemical investigations and catalytic activity measurements on crystallized molydbenum sulfide-cobalt sulfide mixed catalysts. J Catal. 1973;31(2):264-73.

[20] Candia R, Clausen B, Topsøe H. The origin of catalytic synergy in unsupported Co@Mo HDS catalysts. J Catal. 1982;77(2):564-6.

[21] Xing Y, Deng J, Li S, Yue H, Meng R , Gao P. Cutting performance and wear characteristics of Al_2O_3/TiC ceramic cutting tools with WS_2/Zr soft-coatings and nano-textures in dry cutting. Wear. 2014;318:12-26

[22] Watanabe S, Noshiro J, Miyake S. Tribological characteristics of WS_2/MoS_2 solid lubricating multilayer films. Surf Coat Technol. 2004;183:347-51.

[23] Xu X, Rout CS, Yang J. Freeze-dried WS_2 composites with low content of graphene as high-rate lithium storage materials. J MaterChem A. 2013;1:14548-54.

[24] Bhandavat R, David L, Singh G. Synthesis of surface-functionalized WS_2 nanosheets and performance as Li-Ion battery anodes. J PhysChem Lett. 2012;3(11):1523-30.

[25] Feng C, Huang L, Guo Z. Synthesis of tungsten disulfide (WS_2) nanoflakes for lithium ion battery application. Electrochem Comm. 2007;9:119-22.

[26] Chianelli RR, Daage M, Ledoux MJ. Fundamental studies of transition-metal sulfide catalytic materials. Adv Catal. 1994;40:177-232.

[27] Yamada M. Surface fine structure of hydrodesulfurization catalysts. New aspects of promoting effects of Co and Ni. Catal Surv Japan. 1999;3:3-15.

[28] Thakur S, Delmon B. The role of group VIII metal promoter in MoS_2 and WS_2 hydrotreating catalysts: I. ESR studies of Co@Mo, Ni@Mo, and Ni@W catalysts. J Catal. 1985;91(2):308-17.

[29] Ishihara A, Itoh T, Hino T, Nomura M, Qi PY, Kabe T. Effects of solvents on deep hydrodesulfurization of benzothiophene and dibenzothiophene. J Cataly. 1993;140:184-9.

[30] Peng Y, Meng Z, Zhong C, Lu J, Yu W, Yang Z, Qian Y. Hydrothermal synthesis of MoS_2 and its pressure-related crystallization. J Solid State Chem. 2001;159:170-3.

[31] Peng YY, Meng ZY, Zhong C, Lu J, Yu WC, Jia YB, Qian YT. Hydrothermal synthesis and characterization of single-molecular-layer MoS_2 and $MoSe_2$. Chem Lett. 2001;30(8):772-7.

[32] Li WJ, Shi EW, Ko JM, Chen ZZ, Ogino H, Fukuda T. Hydrothermal synthesis of MoS_2 nanowires. J Cryst Growth. 2003;250:418-22.

[33] Devers E, Afanasiev P, Jouguet B, Vrinat M. Hydrothermal syntheses and catalytic properties of dispersed molybdenum sulfides. Catal Lett. 2002;82:13-7.

[34] Rueda N, Bacaud R, Vrinat M. Highly dispersed, nonsupported molybdenum sulfides. J Catal. 1997;169:404-6.

[35] Afanasiev P, Xia G F, Berhault G, Jouguet B, Lacroix M. Surfactant-assisted synthesis of highly dispersed Molybdenum sulfide. Chem Mater. 1999;11(11):3216-9.

[36] Bezverkhy I, Afanasiev P, Lacroix M. Aqueous preparation of highly dispersed molybdenum sulfide. Inorg Chem. 2000;39(24):5416-7.

[37] Genuit D, Afanasiev P, Vrinat M. Solution syntheses of unsupported Co(Ni)–Mo–S hydrotreating catalysts. J Catal. 2005;235(2):302-17.

[38] Nava H, Ornelas C, Aguilar A, Berhault G, Fuentes S, Alonso G. Cobalt-molybdenum sulfide catalysts prepared by in Situ activation of bimetallic (Co-Mo) alkylthiomolybdates. Catal Lett. 2003;86(4):257-65.

[39] Alonso G, Berhault G, Aguilar A, Collins V, Ornelas C, Fuentes S, Chianelli RR. Characterization and HDS activity of mesoporous MoS_2 catalysts prepared by in situ activation of tetraalkylammonium thiomolybdates. J Catal. 2002;208:359-69.

[40] Perkins FK, Friedman AI, Cobas E, Campbell PM, Jernigan GG, Jonker BT. Chemical vapor sensing with monolayer MoS_2. Nano Lett. 2013;13(2):668-73.

[41] Coleman JN, Lotya M, O'Neill A, Bergin SD, King PJ, Khan U, Young K, Gaucher A, De S,. Smith RJ, Shvets IV, Arora SK, Stanton G, Kim HY, Lee K, Kim GT, Duesberg GS, Hallam T, Boland JJ, Wang JJ, Donegan JF, Grunlan JC, Moriarty G, Shmeliov A, Nicholls RJ, Perkins JM, Grieveson EM, Theuwissen K, McComb DW, Nellist PD, Nicolosi V. Two-dimensional nanosheets Produced by liquid exfoliation of layered materials. Science. 2011;331:568-71.

[42] Fuentes S, Dıaz G, Pedraza F, Rojas H, Rosas N. The influence of a new preparation method on the catalytic properties of CoMo and NiMo sulfides. J Catal. 1988;113:535-9.

[43] Naumann AW, Behan AS. Molybdenum disulfide catalyst and the preparation thereof. US Patent 4,243,554, 6 Jan 1981

[44] Nava H, Pedraza F, Alonso G. Nickel-molybdenum-tungsten sulfide catalysts prepared by in situ activation of tri-metallic (Ni-Mo-W) alkylthiomolybdotungstates. Catal Lett. 2005;99:65-71.

[45] Bocarando J, Huirache AR, Bensch W, Huang ZD, Petranovskii V, Fuentes S, Alonso NG. Unsupported Ni-Mo-W sulphide HDS catalysts with the varying nickel concentration. Appl Catal A. 2009;363:45-51.

[46] Poisot M, Bensch W. Decomposition of tetraalkylammonium thiotungstates characterized by thermoanalysis, mass spectrometry, X-ray diffractometry and scanning electron microscopy. Thermochim Acta. 2007;453:42-51.

[47] An G, Liu Y, Chai Y, Shang H, Liu C. Synthesis, characterization and thermal decomposition mechanism of cetyltrimethyl ammonium tetrathiotungstate. J Natur Gas Chem. 2006;15(2):127-33.

[48] Brito JL, Ilija M, Hernandez P. Thermal and reductive decomposition of ammonium thiomolybdates. Thermochim Acta. 1995;256(2):325-38.

[49] Voorhoeve RJH, Wolters HBM. Tungsten sulfides obtained by decomposition of ammonium tetrathiotungstate Z Anorg Allg Chem. 1970;376:165-79.

[50] Yi Y, Williams CT, Glascock M, Xiong G, Lauterbach J, Liang C. Transformation of Mo and W thiosalts into unsupported sulfide catalysts: A temperature dependent in-situ spectroscopic investigation. Mater Res Bull. 2014;56:54-64.

[51] Prasad RL, Kushwaha A, Szilágyi IM, Kótai L. Solid-state thermal degradation behaviour of 1-D coordination polymers of Ni(II) and Cu(II) bridged by conjugated ligand. J Therm Anal Calorim. 2013;114:653-64.

[52] Szilágyi IM, Deák A, Várhelyi Jr C, Madarász J, Pokol G, Gömöry Á, Várhelyi C. Structural and thermal study of asymmetric α-dioxime complexes of Co(III) with Cl and methyl-pyridines. Polyhedron. 2010;10:2185-9.

[53] Hunyadi H, Sajó I, Szilágyi IM. Structure and thermal decomposition of ammonium metatungstate. J Therm Anal Calorim. 2014;116, 329-37.

[54] Szilágyi IM, Santala E, Heikkilä M, Kemell M, Nikitin T, Khriachtchev L, Räsänen M, Ritala M, Leskelä M. Thermal study on electrospun polyvinylpyrrolidone/ammonium metatungtate nanofibers: Optimising the annealing conditions for obtaining WO_3 nanofibers. J Therm Anal Calorim. 2011;105:73-81.

[55] Szilágyi IM, Madarász J, Király P, Tárkányi G, Tóth AL, Szabó A, Varga-Josepovits K, Pokol G. Stability and controlled composition of hexagonal WO_3. Chem Mater. 2008;20:4116-25.

[56] Madarász J, Szilágyi IM, Hange F, Pokol G. Comparative evolved gas analyses (TG-FTIR, TG/DTA-MS) and solid state (FTIR, XRD) studies on thermal decomposition of ammonium paratungstate tetrahydrate (APT) in air. J Anal Appl Pyrol. 2004;72:197-201.

Figures

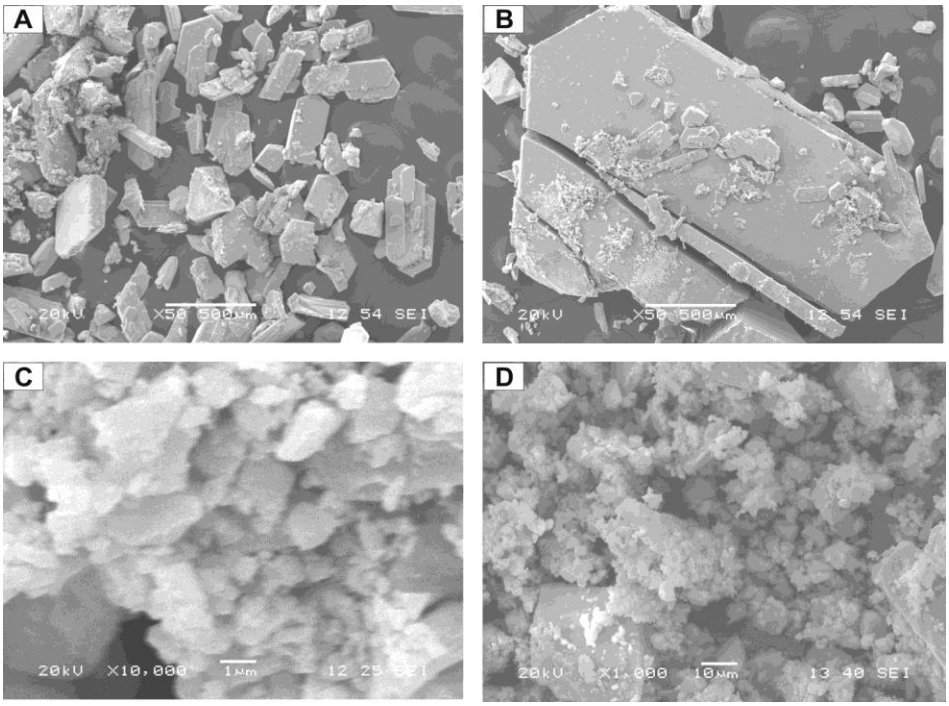

Figure 1. SEM images of the ATT crystals (A, B) and powder (C,D)

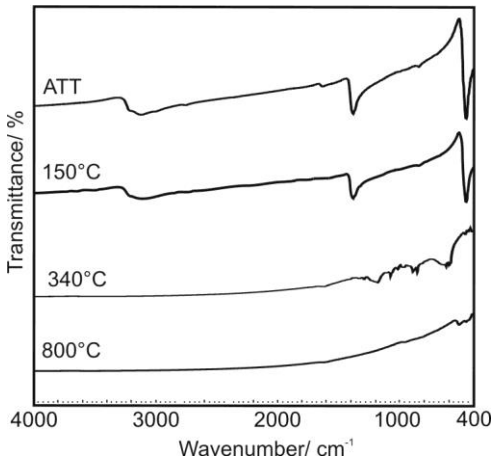

Figure 2. FTIR spectra of the thermal decomposition products of ATT powder in N_2

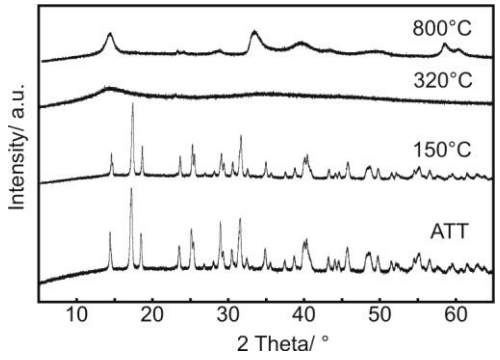

Figure 3. XRD patterns of the thermal decomposition products of ATT powder in N_2

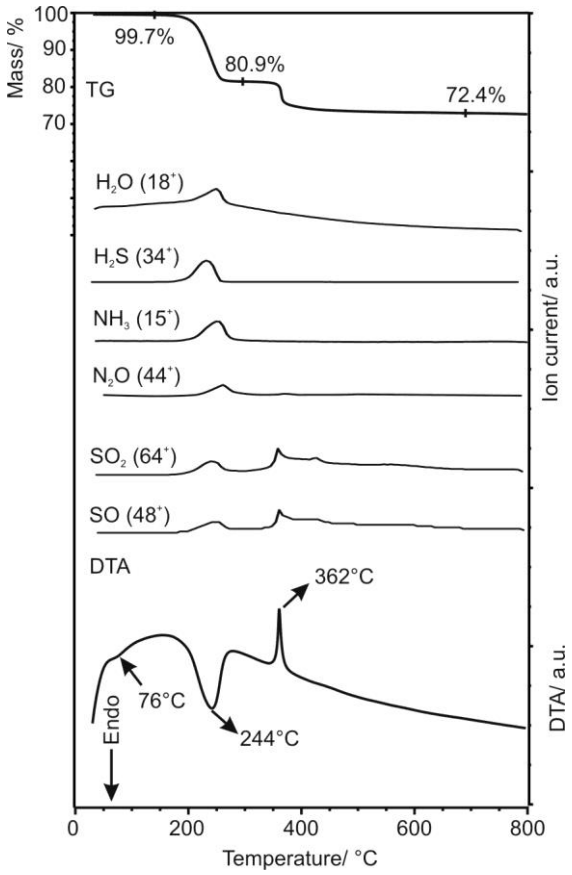

Figure 4. TG/DTA and evolved gas analytical MS ion current curves of the thermal decomposition of ATT powder in N_2

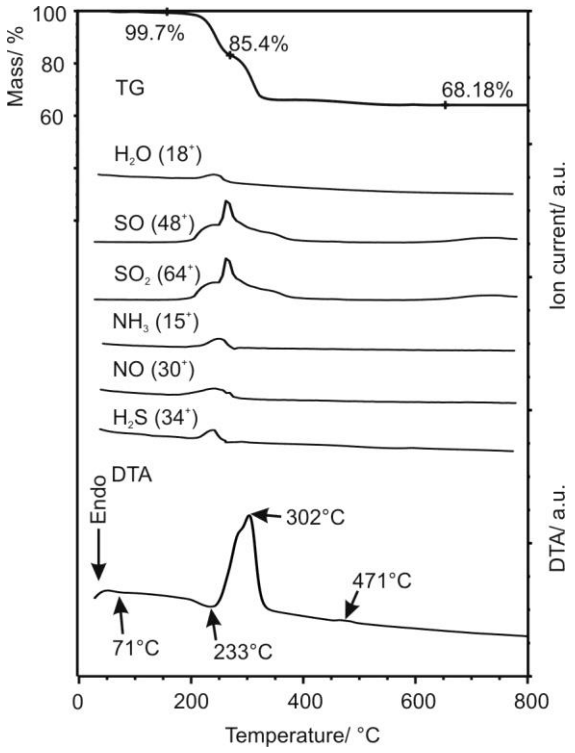

Figure 5. TG/DTA and evolved gas analytical MS ion current curves of the thermal decomposition of ATT powder in air

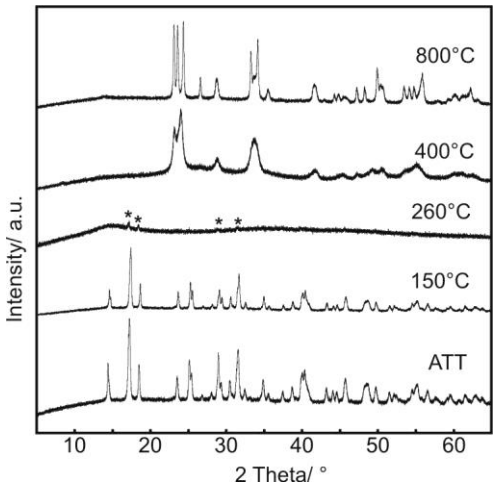

Figure 6. XRD patterns of the thermal decomposition products of ATT powder in air, *: ATT peaks

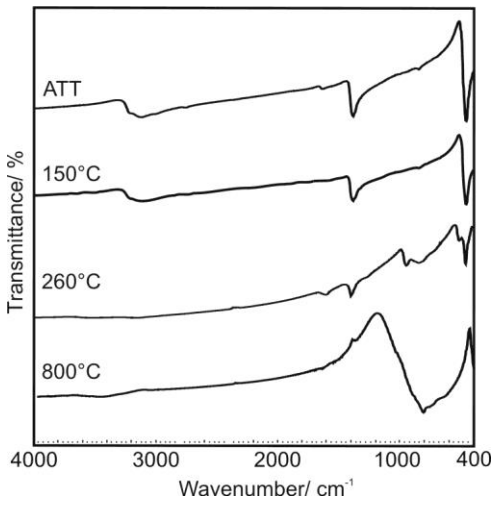

Figure 7. FTIR spectra of the thermal decomposition products of ATT powder in air

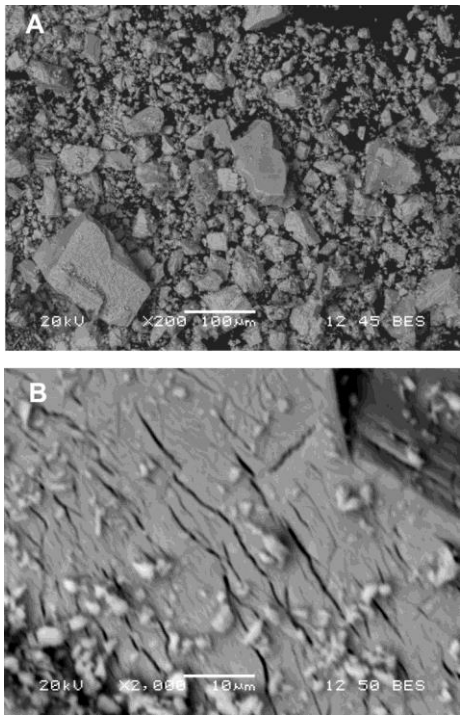

Figure 8. SEM images of the as-obtained mixture at 260°C in air

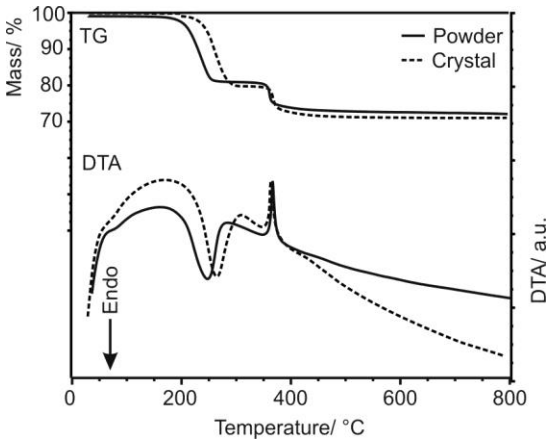

Figure 9. TG/DTA curves of the thermal decomposition of ATT powder and crystals in N_2

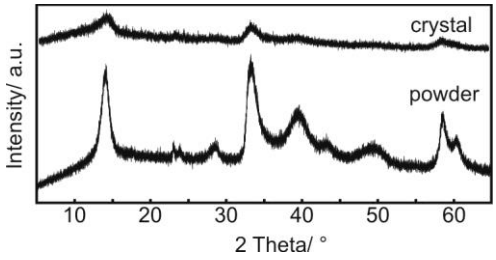

Figure 10. XRD patterns of the as-formed WS_2 form the ATT powder and crystals in N_2 at 800 °C